

Flux penetration into an artificially granular high- T_c superconductor

M. R. Koblichka*

Department of Physics, University of Oslo, Blindern, N-0316 Oslo, Norway

L. Püst†

Department of Physics and Astronomy, Wayne State University, 666 West Hancock, Detroit, Michigan 48202

A. Galkin, P. Nálevka, and M. Jirsa

Institute of Physics, Academy of Sciences of the Czech Republic, Na Slovance 2, CZ-18040 Praha 8, Czech Republic

T. H. Johansen and H. Bratsberg

Department of Physics, University of Oslo, Blindern, N-0316 Oslo, Norway

B. Nilsson and T. Claeson

Physics Department, Chalmers University of Technology, S-41296 Gothenburg, Sweden

(Received 9 February 1998; revised manuscript received 25 August 1998)

A $\text{YBa}_2\text{Cu}_3\text{O}_{7-\delta}$ thin film is patterned into a hexagonal close-packed lattice of disks ($2r = 50 \mu\text{m}$) which are touching each other at the circumferences in order to enable the flow of an intergranular current. Such a sample was suggested by Koblichka *et al.* [Appl. Phys. Lett. **70**, 514 (1997)] as a model for a layered granular structure like in a $(\text{Pb,Bi})_2\text{Sr}_2\text{Ca}_2\text{Cu}_3\text{O}_{10+\delta}$ (Bi-2223) tape. The magnetization measurements reveal an anomalous position of the low-field peak (central peak) similar to Bi-2223 tapes. Magneto-optic imaging is employed to visualize the local-field distributions. At low magnification, the flux patterns in the intergranular area between the disks are observed. The observations at high magnification reveal the flux penetration and pinning within the disks. It is shown that such samples may serve as model samples for granular high- T_c superconductors. [S0163-1829(99)05617-9]

I. INTRODUCTION

Properties of granular samples are important to be understood in detail, as most future applications will involve high- T_c superconductors with a certain amount of granularity, be it $(\text{Pb,Bi})_2\text{Sr}_2\text{Ca}_2\text{Cu}_3\text{O}_{10+\delta}$ (Bi-2223) tapes for power applications or bulk, melt-processed $\text{YBa}_2\text{Cu}_3\text{O}_{7-\delta}$ (YBCO) for levitation. Recently, in silver-sheathed Bi-2223 tapes some anomalous features in the magnetic properties were observed, including an anomalous position of the low-field peak in magnetization loops (MHL's) at *positive* fields in decreasing positive external field¹⁻³ and a pronounced asymmetry of the magnetization loops.⁴ These features are also reflected in a hysteresis of the transport currents in applied fields.⁵

Hard type-II superconductors always exhibit a low field peak in the MHL's, which is a result of a field dependent current density.⁶ Within the framework of the critical state model, the position of this peak B_{pc} in decreasing external field is expected to be located at zero or slightly *negative* fields depending on the aspect ratio r/d of the sample (where r denotes the sample radius and d the thickness). This is also valid in perpendicular geometry, i.e., for the field applied perpendicular to the surface of a thin sample as shown in Ref. 7. A positive B_{pc} , however, cannot be explained by any critical state model. To attempt an explanation of this feature, effects of granularity have to be considered. From magnetic measurements on tapes after bending to a very small diameter, which effectively breaks the contacts between the grains,^{2,4} it was learned that the intergranular currents are

responsible for the anomalous peak position. In Ref. 1, we proposed a model which describes a layer of grains within a tape as a lattice of densely packed superconducting thin disks which touch each other at the circumferences in order to enable the flow of transport (= intergranular) currents. In decreasing external field, the local field at the circumference of each disk becomes negative before the direction of the applied field is reversed. The transport currents will experience this negative field when passing a connection between the disks. This should lead to the experimentally observed situation that the local field B_i is apparently ahead of the external field B_e and consequently $B_{pc} > 0$. In order to prove this model approach, we proposed a model sample to be fabricated.¹

In this paper, we present magnetic and magneto-optic measurements on a model sample which realizes the proposed structure. The parameters of this sample were selected so that the contributions of the intragranular currents (within the disks) and of the intergranular currents (between the disks) to the total magnetic moment are approximately equal. YBCO was chosen as superconductor because such films can be prepared and patterned in excellent quality. Furthermore, the superconducting properties of YBCO are close enough to Bi-2223 tapes ensuring the possibility for measurements in a wide temperature range. In Fig. 1(a), a schematic drawing of this structure is shown, giving the definition of the contact width w between the disks. The arrows denote the current flow of the inter- and intragranular currents through the sample.

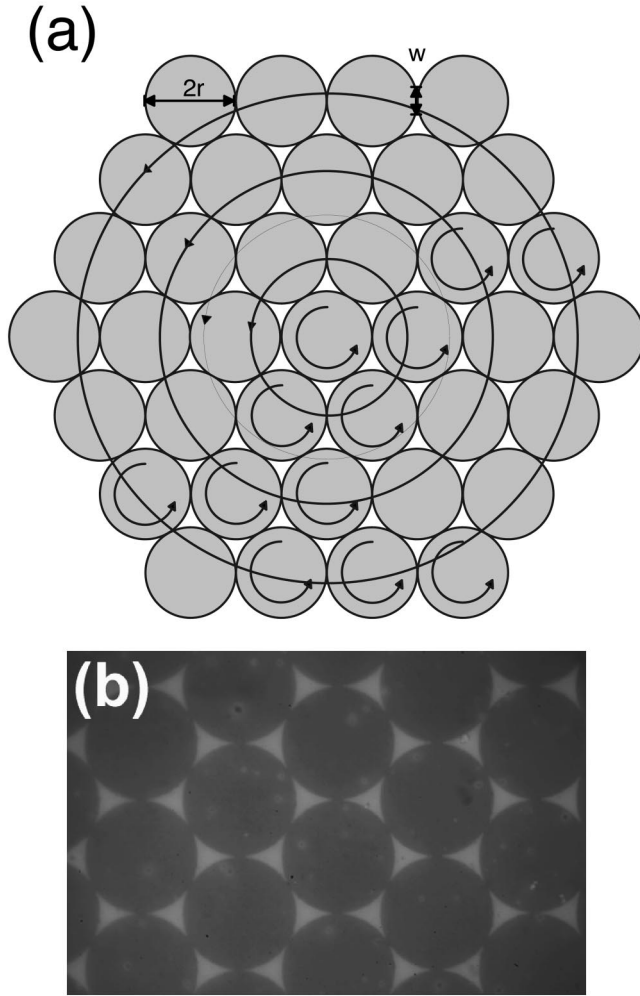


FIG. 1. (a): Schematic drawing of the model sample as proposed in Ref. 1, consisting of a hexagonally close-packed lattice of superconducting disks with radius r . Also shown is the definition of the contact width w between the disks. A polarization image of patterned YBCO thin film is presented in (b). The pattern shows the excellent etching of the structure which ensures a uniform current flow through the connections between the disks. The diameter of a disk is $50 \mu\text{m}$, the contact width $3.5 \mu\text{m}$.

As a tool to investigate the properties of the model sample we have chosen magnetization loops (MHL's) and magneto-optic (MO) imaging,⁸ which allows the measurement of the local-field distributions. This technique is known as a powerful method to study effects of granularity in superconductors; recent investigations were carried out on YBCO ceramics,⁹ bulk $\text{Bi}_2\text{Sr}_2\text{CaCu}_2\text{O}_{8+\delta}$ ceramics,¹⁰ and Bi-2223 tapes.¹¹ In the present case, it allows us to observe the flux behavior on various length scales thus revealing the inter- and intragranular properties of the sample. The magneto-optic visualization techniques based on the Faraday effect combine a relatively high spatial resolution with the unique possibility to observe dynamic processes.⁸

This paper is organized as follows: In Sec. II, we outline briefly some details of the MO imaging technique, and details of the sample preparation. Section III A presents the results of the magnetic measurements, which indicate that the model sample is capable of reproducing features found in the MHL's of Bi-2223 tapes. In Sec. III B, we present the

local flux distributions of the model sample at low (entire sample) and high magnification (individual disks). At low magnification, we observe the flux distribution in the intergranular are between the disks. The local measurements demonstrate that the model sample indeed works as predicted by our model. Finally, in Sec. IV some conclusions are drawn.

II. EXPERIMENTAL PROCEDURE

The field distributions are obtained by the rotation of the polarization plane of linearly polarized light which passes a magneto-optically active layer exposed to the magnetic field of the underlying superconductor. From flux-free regions the light is reflected without rotation and thus cannot pass the analyzer which is set in a crossed position with respect to the polarizer. The images presented here are therefore maps of the z component of the local magnetic field $B_{i,z}$. As MO active layer, we use a Bi-doped yttrium-iron-garnet film with in-plane anisotropy. The microscope provides a uniform light field and a heat filter which ensures that the heat load on the sample is negligible. The images are recorded using an 8-bit Kodak DCS 420 charge-coupled device (CCD) digital camera (each image consists of 1536×1024 pixels per frame) and subsequently transferred to a computer for processing and storage. In the magneto-optic apparatus the sample was mounted on the cold finger of an optical Helium flow cryostat.¹² The sample was glued onto a copper holder using conductive carbon cement¹³ to ensure a good thermal contact, and the indicator film is laid on the sample surface and centered. The magnetic field was applied perpendicular to the sample surface (i.e., along the c axis of the YBCO) using a copper solenoid with $B_{e,\text{max}} = \pm 120$ mT. The magnetization measurements were performed using a vibrating sample magnetometer (VSM) PAR Model 155 with a maximum field of ± 2 T, also with $B_e \parallel c$.

The sample was prepared by means of laser ablation on a LaAlO_3 substrate. The thickness of the YBCO thin film is 150 nm. A structure of hexagonally close-packed circular disks is then patterned by means of electron-beam lithography. The diameter of the disks, $2r$, is $50 \mu\text{m}$, and the contact width $w = 3.5 \mu\text{m}$. The sample has an overall size of $4 \times 4 \text{mm}^2$, comprising ≈ 8000 disks. The transition temperature T_c after the patterning process is about 83 K. In Fig. 1(b), a polarization image of our structure is presented. The pattern shows the excellent etching of the structure which ensures a uniform current flow through the connections between the disks.

III. RESULTS AND DISCUSSION

A. Magnetic properties

First, we discuss the magnetic properties of our model sample. Full magnetization loops were measured in the temperature range $5 \leq T \leq 70$ K as presented in Fig. 2. The loops reveal that the peak position of the central peak is indeed anomalously located on the positive side as predicted by our model. Above 50 K, the peak position is very close to 0 T, but on decreasing temperature, the peak position becomes increasingly positive. From these MHLs, the positions of the low-field peak B_{pc} are extracted on the decreasing field

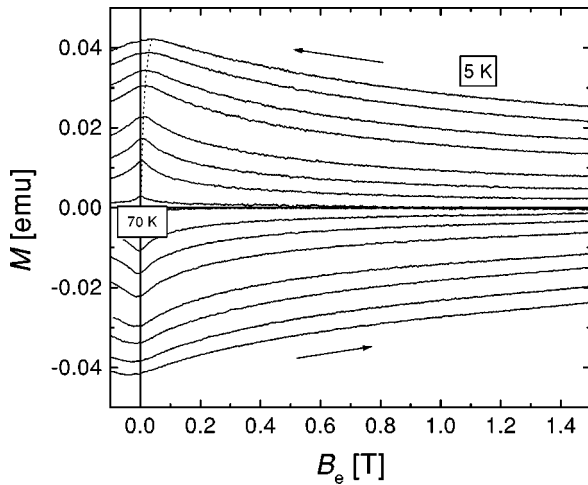


FIG. 2. Full magnetization loops of the model sample, measured at 5, 10, 15, 20, 30, 40, 50, and 70 K. The other temperatures are omitted for clarity. The arrows denote the direction of measurement. The dashed line indicates the temperature behavior of the peak position B_{pc} .

branch. In Fig. 3, B_{pc} is plotted as a function of temperature together with peak positions derived from MHL's of a monofilamentary Bi-2223 tape¹ and an homogeneous YBCO thin film, which does not show any structural defects as proved by MO imaging.¹⁴ It is clearly visible that our model sample exhibits the low-field peak at *positive* fields like the Bi-2223 tape; at $T = 5$ K the maximum is located at $B_{pc} = +38$ mT. Above 20 K, the peak positions of the model sample and of the monofilamentary tape are similar. Also the multifilamentary tape with 19 filaments exhibits the anomalous behavior of the peak. Both tapes show a strongly developed anomalous peak position at low temperatures, being as large as +170 mT at $T = 3.4$ K for the monofilamentary tape. This is attributed to a strong increase of the intragranular currents at low temperatures leading to a truly granular behavior, i.e., the intragranular currents are much larger than

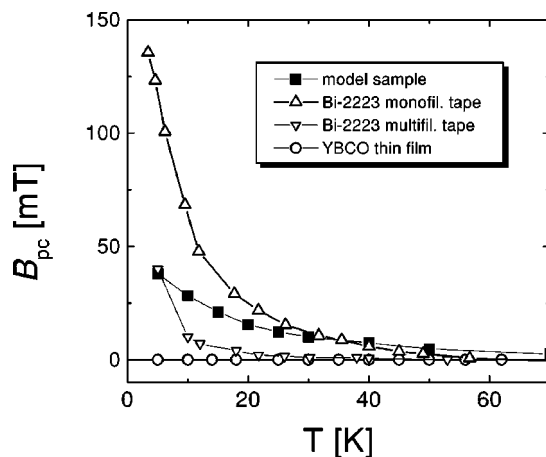


FIG. 3. The positions of the central peak in magnetization loops B_{pc} of our model sample as function of temperature. Also shown are the peak positions of a monofilamentary Bi-2223 tape (data taken from Ref. 1), a multifilamentary Bi-2223 tape comprising 19 filaments (Ref. 25), and a homogeneous YBCO thin film for comparison.

the intergranular ones.¹⁵ In contrast to this, the low-field peak of the homogeneous YBCO thin film is always located at 0 T as expected from the critical state models.^{6,7} This shows that our model sample is capable of reproducing non-trivial features in the behavior of layered granular structures like a Bi-2223 tape. However, not all properties of the MHL's obtained up to now on Bi-2223 tapes are reproduced; namely the pronounced asymmetry of the MHL's.⁴

B. Flux distributions

All flux patterns presented in this paper are taken at a temperature $T = 18$ K in order to achieve large enough contrasts; the exposure time of the camera is always kept constant during an experimental run in order to allow for a direct comparison of the images to each other. Flux is imaged as bright areas; well-shielded regions are represented as dark.

An MO flux pattern is presented in Fig. 4, using a low magnification. In Fig. 4(a), an external magnetic field $B_e = 6$ mT is applied to the zero-field cooled sample. The arrows are pointing to a defect (scratch) in lower part of the sample, where vortices are able to penetrate into the structure more easily than in the remainder of the sample. Note that along the sample edges, a field overshoot (i.e., the local field $B_{i,z}$ is larger than the applied field B_e) can be observed, which is characteristic for a superconductor with a large demagnetization factor. However, the low intensity detected along the sample edges in our case (as compared to an homogeneous thin film of the same size) is an indication of a relatively small current density induced in the sample. Furthermore, flux is entering the structure starting from the sample edges, so a flux front can be observed. This is a quite surprising observation, revealing that vortices exist in the intergranular area, thus forming an ‘‘effective medium.’’ This flux pattern is evidently due to the intergranular currents.

In Fig. 4(b), the external magnetic field is raised to 18 mT. Flux seems to enter the sample as if the sample would be completely homogeneous. However, a closer inspection of the images reveals important differences, as the domains of entering flux have some internal structure. In order to clarify this behavior, we investigated parts of the sample using a higher magnification (see Fig. 5). Here it is very important to point out that the penetrating vortices generate a set of characteristic current discontinuity lines (d lines).¹⁶ The schematical drawing in Fig. 4(c) presents the ideal geometric pattern of the d^+ lines in a sample without structural defects. This ideal geometric shape of the d^+ lines in our model sample is disturbed by the presence of a defect at the bottom of the image, where two bright d^- lines can be seen [Fig. 4(b)].

As the concept of d lines¹⁶ in the current flow of type-II superconductors is very important for the interpretation of our observations, we just recall in the following some characteristic properties of the d lines as described in Ref. 16: (i) The so-called d^+ lines are formed where the currents are forced to make a sharp turn in order to flow parallel to the sample edges and appear in the MO images as dark lines in increasing external field, and as bright lines in decreasing field. The d^- lines are generated along the sample edges (= field overshoot due to demagnetization effects) and along

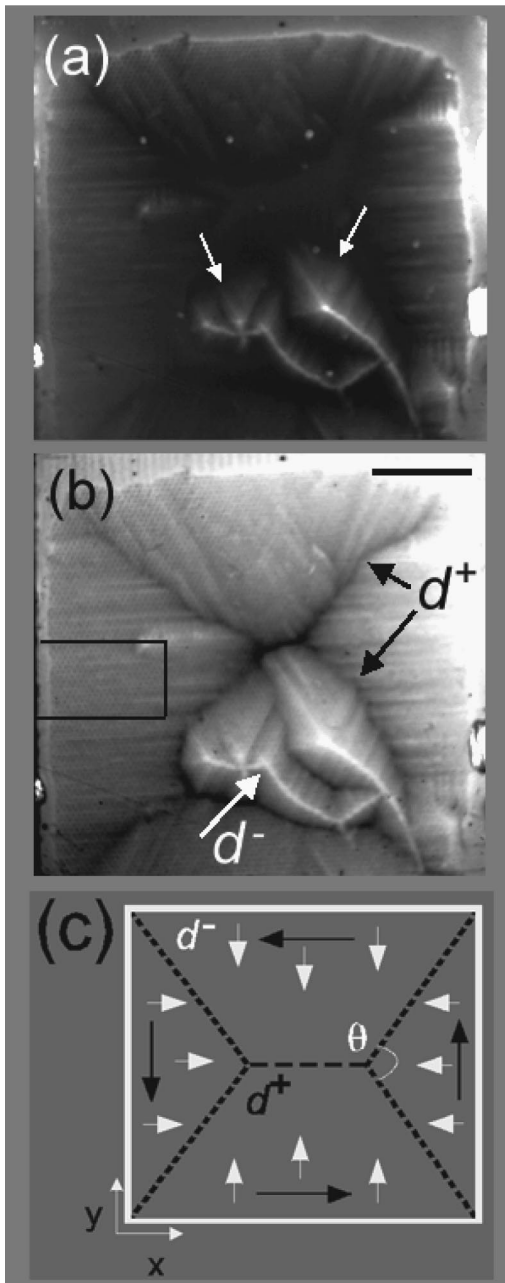


FIG. 4. Flux distributions of the model sample at $T = 18$ K, taken at low magnification to show the properties of the entire sample. (a): $\mu_0 H_a = 6$ mT. The arrows denote a defect (scratch) in the structure, which leads to additional flux penetration. The marker is 1 mm long. (b): $\mu_0 H_a = 18$ mT revealing the pattern caused by the intergranular currents. The characteristic, dark d^+ lines (see text) clearly reflect the flow of the intergranular currents through the entire sample. Bright d^- lines are visible along a defect in the lower part of the image, and along the sample edges (demagnetization effect). The black frame shows the region observed with higher magnification in Fig. 5(c) presents a schematic drawing of the position of the d^+ and d^- lines in an undisturbed, homogeneous case. As described in the text, the d lines act like a skeleton for the flux penetration. The black arrows in (c) denote the flow of the currents; the white arrows indicate the direction of flux penetration. The angle Θ between the d^+ lines gives information about the currents in x and y directions via $j_y/j_x = \tan(\Theta/2)$. Therefore the observation of d lines in the intergranular area (“effective medium”) is a strong evidence that the observed flux pattern is due to the intergranular currents only.

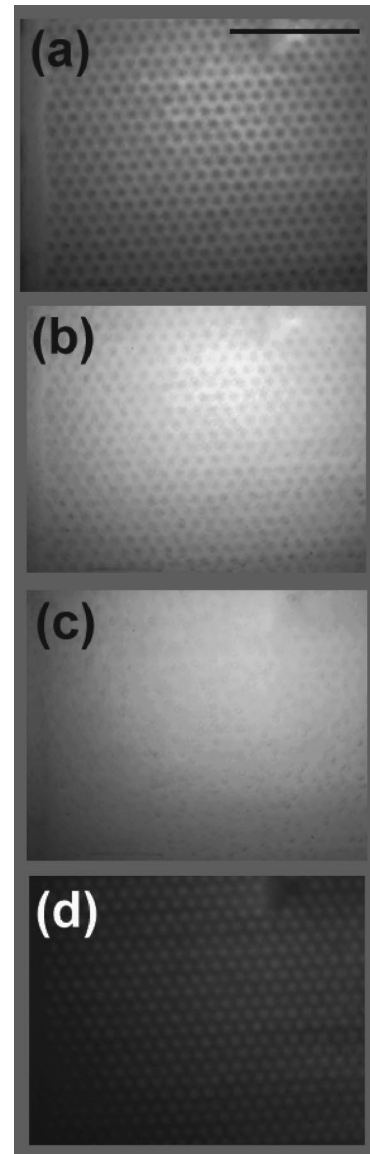


FIG. 5. Magneto-optic images of the sample using a higher magnification; the marker is $500 \mu\text{m}$ long. (a) $B_e = 18$ mT after zero-field cooling. The flux can be seen penetrating the sample through channels between the disks. (b) $B_e = 45$ mT. The individual disks still appear as dark spots, but the flux has already started to penetrate into the outer rim of the disks. (c) is taken after reduction of the external magnetic field from 45–39 mT. A nearly homogeneous gray pattern results (see text). (d) shows the remanent state generated after reduction of the external field to 0 mT. Vortices are observed being pinned *within* the disks. Annihilation effects are leading to a dark rim along the sample edge; even vortices inside some disks along the sample edges are annihilated.

structural defects which facilitate the flux penetration process;¹⁷ these lines appear as bright lines in increasing field; their intensity depends on the demagnetization factor of the sample and on the induced current density. (ii) The location of the d^+ lines is determined by the whole sample geometry. In particular, differences in the critical current densities in different regions of the sample were found to contribute strongly to the appearance of d^+ lines; thus the anisotropy of the currents within the observation plane can be determined by means of the angle Θ [see Fig. 4(c)].^{18,19}

Therefore we can state that the d^+ lines *reflect the magnetic behavior of the entire sample*. (iii) The flux lines are not able to cross the d^+ lines during flux penetration processes. This is a very general result following from many MO observations in literature.⁸ This behavior is illustrated in Fig. 4(c). The flux penetrating the sample starting from the edges can only move *towards* the d^+ line, but is never able to cross it due to the different direction of the induced currents. Thus the d^+ lines divide the superconductor into independent areas of flux motion and their observation determines a quasi-skeleton of the flux behavior. (iv) The d^+ and d^- lines do not change their position or intensity while lowering or reversing the external magnetic field, although the magneto-optically detected intensities of the d^+ and d^- lines are reversed in the remanent state.¹⁶ Furthermore, the d^+ lines depend on the d^- lines, thus allowing the determination of any differences in current density inside a superconducting sample as demonstrated in Refs. 18 and 20. Therefore the appearance of the dark d^+ lines [Fig. 4(b)] in the “effective medium” between the disks proves unambiguously that we indeed observe a flux pattern generated exclusively by the intergranular (transport) currents induced in our model sample.

If we compare this kind of flux distribution to those obtained on Bi-2223 tapes, many similarities are found with flux patterns obtained at elevated temperatures ($T > 50$ K). The flux patterns at such elevated temperatures were found to be practically uniform, and do not reveal any traces of granularity as observed at low temperatures. As an explanation, it was argued that the flux patterns are mainly due to the intergranular currents, with a negligible contribution of the intragranular currents.^{15,21} Our results on the model sample now confirm this explanation. Even at low temperatures, where effects of granularity are important, a dark d^+ line can be observed in the center of the tapes as shown in Refs. 15 and 21. This indicates that even at low temperatures, where the intragranular current density is very large, also large transport current can flow in such a tape.

To investigate the behavior of individual disks (= grains) in detail, a higher magnification was used for the series of images presented in Figs. 5(a)–(d). The selected area is marked in Fig. 4(b); on the left side of the image the edge of the sample is visible. In Fig. 4(a), a field of 18 mT is applied. At this higher magnification, the behavior of the individual disks can be observed. The flux enters the sample through the effective medium (intergranular area). At this field, the flux penetrates only into the outer rim of each disk, as shown in the flux profiles of Fig. 7 below. At an applied field of 45 mT [Fig. 5(b)], the disks can still be recognized having a dark spot in the center. The current density inside the disks is evidently much larger than the intergranular current density, similar to most real granular high- T_c samples.

Figure 5(c) presents the flux pattern after decreasing the external magnetic field from 45–39 mT. Note that the flux pattern appears to be nearly uniformly gray. When reducing the external magnetic field, vortices leave the effective medium quite easily due to the low pinning. This reduces the local field $B_{i,z}$ in the channels between the disks. Furthermore, inside the disks, which were just close to the full penetration field B^* , the vortices also rearrange according to the Bean model for perpendicular geometry.^{22–24} The center of

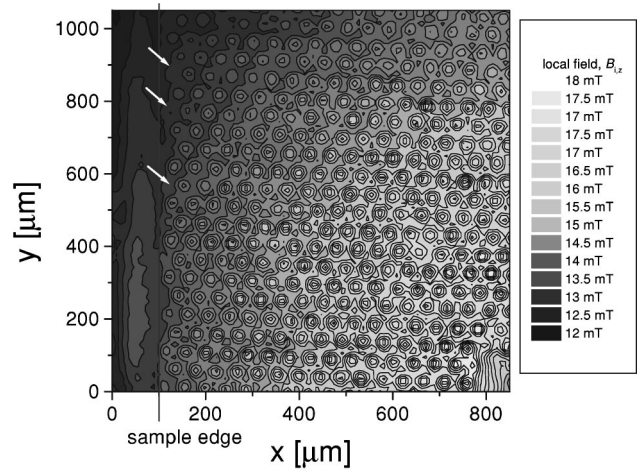


FIG. 6. Contour plot of the local flux density $B_{i,z}$ in the remanent state ($B_e = 0$ T), after applying 45 mT. This plot corresponds directly to the calibrated magneto-optic image shown in Fig. 5(d). The edge of the sample is indicated by a black line. The arrows point to some disks, where even the trapped vortices are already annihilated by invading vortices of opposite polarity.

each disk (which represents the d line in circular geometry) becomes bright, while at the disk circumferences the vortices leave the sample. This double process causes then the uniformly gray flux pattern in accordance with theory. A condition for the observation of such a uniformly gray flux pattern is that the magnitude of the inter- and intragranular current densities is not too different from each other. Indeed, in Bi-2223 tapes after bending to a small diameter, which effectively reduces the intergranular current density, also such a uniformly gray flux pattern is observed upon reduction of the external magnetic field.

The final remanent state ($B_e = 0$ T) is presented in Fig. 5(d). Pinned vortices can be observed being trapped inside the disks; see also the flux profile in Fig. 7 below. Along the channels between the disks, most vortices have disappeared. Vortices of opposite polarity can easily invade the sample and annihilate with the trapped vortices. In some disks along the sample edge, also, the vortices trapped inside the disk have already disappeared. All this is an indication that the minimum of the vortex density occurs when still a small positive field is applied, i.e., the position of the central peak in a magnetization loop is located at *positive* field. From these observations, it is possible to confirm that the model sample indeed works as predicted in Ref. 1.

Figure 6 presents a contour plot of the local flux density $B_{i,z}$ in the remanent state. This plot directly corresponds to the calibrated MO image shown in Fig. 5(d). From this representation it is clearly visible that vortices are trapped inside the disks. Only very close to the sample edge, some disks do not have trapped vortices in them (white arrows). This plot also confirms that the stray field around a disk causes a low flux density just in the contact areas between the disks (note, i.e., the black spots denoting the field minima between the disks), as predicted in the model of Ref. 1. The transport currents experience, therefore, a much lower field as in the case of a homogeneous sample. As the applied field was only raised to 45 mT, the stray field around the disks is not yet of opposite sign. This would require larger applied fields, lead-

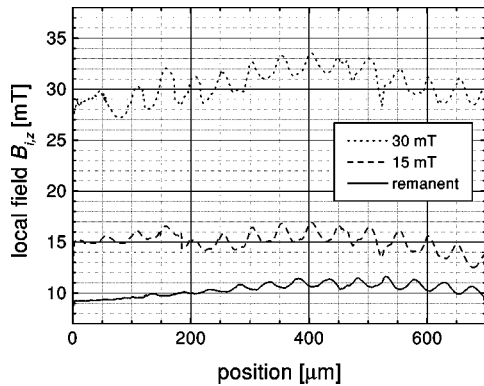


FIG. 7. Flux density profiles for 15 and 30 mT applied field and for the remanent state as shown in Fig. 6. Note that the uniformity and excellent quality of our model structure is reflected by the identical flux density gradients in each disk. The minima in the case of applied field correspond exactly to the maxima measured in the remanent state. The profiles also reveal that the contribution of the intragranular currents is just superimposed on the flux profile caused by the transport currents.

ing to a higher density of trapped vortices. This behavior will be investigated in detail in a subsequent paper.²⁶

In Fig. 7, flux density profiles are presented for 15 and 30 mT applied field and for the remanent state. From these profiles, several important points can be revealed: The uniformity and excellent quality of our model structure is reflected by the identical distances between the maxima (or minima) and by the identical flux density gradients in each disk. The minima in the case of applied field correspond exactly to the maxima measured in the remanent state. The profiles also reveal that the contribution of the intragranular currents is just superimposed on the flux profile caused by the transport currents. From the gradients of the inter- and intragranular area, we can determine the inter- (j_c^T) and intragranular (j_c^G) current density by means of the procedure described in Ref. 12, taking into account the respective size. The two contributions j_c^G and j_c^T can be obtained from the flux profiles. j_c^T is quite small (2.0×10^7 A m⁻², at $B_e = 15$ mT) and depends

on the applied field, whereas j_c^G is about one order of magnitude larger (1.7×10^8 A m⁻²) and practically not affected by the external magnetic field.

The MO flux patterns demonstrate that the model sample indeed works as predicted in our model of Ref. 1. This will enable us to future experiments with modified sample parameters (diameter of disks, contact width w , intragranular current density) in order to model the behavior of various granular high- T_c samples, especially the properties of Bi-2223 tapes.

IV. CONCLUSIONS

In conclusion, we have prepared a YBCO thin film with artificial granularity, which was suggested as model sample to exhibit some properties of Bi-2223 tapes. Flux patterns of this sample were studied by means of magneto-optic imaging revealing the penetration of flux into the effective medium *between* the disks. The magnetization measurements and the MO images clearly demonstrate that such a YBCO thin film with artificial granularity may serve as a model sample for granular high- T_c superconductors. The present model sample reproduces already several features found in Bi-2223 tapes; especially the anomalous peak position of the low-field peak in the magnetization loops. This will enable us to future experiments with modified sample parameters (diameter of disks, contact width w , intragranular current density) in order to model the behavior of different granular high- T_c samples.

ACKNOWLEDGMENTS

Valuable discussions with Y. Galperin (Oslo), A. A. Polyanskii (Madison), and J. R. Clem (Iowa) are gratefully acknowledged. We thank Y. Shen and P. Vase (NST A/S, Brøndby, Denmark) for the homogeneous YBCO thin film and the various Bi-2223 tapes used for comparison, and V. Gregor and S. Danis (ASCR, Prague) for technical assistance. This work was supported by The Research Council of Norway; the work in Prague was supported by Grant No. A1010512 of GA ASCR. L.P. acknowledges support from NATO by Grant No. 961357.

*Present address: Superconductivity Research Laboratory, International Superconductivity Technology Center, 1-16-25, Shibaura, Minato-ku, Tokyo 105, Japan.

†Present address: Seagate Technologies, Bloomington, MN 55435.

¹M. R. Koblischka, L. Püst, A. Galkin, and P. Nálezka, *Appl. Phys. Lett.* **70**, 514 (1997).

²K.-H. Müller, C. Andrikis, and Y. C. Guo, *Phys. Rev. B* **55**, 630 (1997).

³M. R. Cimberle, C. Ferdeghini, R. Flükiger, E. Giannini, G. Grasso, D. Marrè, M. Putti, and A. S. Siri, *Physica C* **251**, 61 (1995).

⁴P. Nálezka, M. Jirsa, L. Püst, A. Galkin, M. R. Koblischka, and R. Flükiger, in *Applied Superconductivity*, Proceedings of the Third European Conference on Applied Superconductivity, edited by H. Rojalla and D. H. A. Blank, IOP Conf. Proc. No. 158 (Institute of Physics, Bristol, 1997), pp. 1161–1164.

⁵L. Cesnak, T. Melišek, P. Kováč, and I. Hušek, *Cryogenics* **37**, 823 (1997).

⁶H. Ullmaier, *Irreversible Properties of Type-II Superconductors*

(Springer-Verlag, Berlin, 1975).

⁷E. H.Brandt, *Phys. Rev. Lett.* **78**, 2208 (1997); T. B. Doyle, R. Labusch, and R. A. Doyle, *Physica C* **290**, 148 (1997).

⁸M. R. Koblischka and R. J. Wijngaarden, *Supercond. Sci. Technol.* **8**, 199 (1995).

⁹N. Moser, M. R. Koblischka, and H. Kronmüller, *J. Less-Common Met.* **164-165**, 1308 (1990); M. R. Koblischka, Th. Schuster, and H. Kronmüller, *Physica C* **211**, 263 (1993); **219**, 205 (1994); J. Albrecht, Ch. Jooss, R. Warthmann, A. Forkl, and H. Kronmüller, *Phys. Rev. B* **57**, 10 332 (1998).

¹⁰M. R. Koblischka, S. L. Huang, T. H. Johansen, H. Bratsberg, and K. Fosheim, *Physica C* **282-287**, 1469 (1997).

¹¹U. Welp, D. O. Gunter, G. W. Crabtree, W. Zhong, U. Balachandran, P. Haldar, R. S. Sokolowski, V. K. Vlasko-Vlasov, and V. I. Nikitenko, *Nature (London)* **276**, 44 (1996); U. Welp, D. O. Gunter, G. W. Crabtree, J. S. Luo, V. A. Maroni, W. L. Carter, V. K. Vlasko-Vlasov, and V. I. Nikitenko, *Appl. Phys. Lett.* **66**, 1270 (1995); A. E. Pashitski, A. A. Polyanskii, A. Gurevich, J. A. Parrell, and D. C. Larbalestier, *Physica C* **246**, 133 (1995);

- Appl. Phys. Lett. **67**, 2720 (1995); J. A. Parrell, A. A. Polyanskii, A. E. Pashitski, and D. C. Larbalestier, Supercond. Sci. Technol. **9**, 393 (1996); Th. Schuster, H. Kuhn, A. Weisshardt, H. Kronmüller, B. Roas, O. Eibl, M. Leghissa, and H.-W. Neumüller, Appl. Phys. Lett. **69**, 1954 (1996); A. E. Pashitski, A. Gurevich, A. A. Polyanskii, D. C. Larbalestier, A. Goyal, E. D. Specht, D. M. Kroeger, J. A. DeLuca, and J. E. Tkaczyk, Science **275**, 367 (1997).
- ¹²T. H. Johansen, M. Baziljevich, H. Bratsberg, Y. Galperin, P. E. Lindelof, Y. Shen, and P. Vase, Phys. Rev. B **54**, 16 264 (1996).
- ¹³Conductive Carbon Cement (CCC), Neubauer Chemikalien, D-48021 Münster, Germany.
- ¹⁴M. R. Koblishka, T. H. Johansen, H. Bratsberg, L. Püst, Y. Shen, and P. Vase, J. Phys. C **9**, 10 909 (1997).
- ¹⁵M. R. Koblishka, T. H. Johansen, H. Bratsberg, and P. Vase, Supercond. Sci. Technol. **12**, 113 (1999).
- ¹⁶Th. Schuster, M. V. Indenbom, M. R. Koblishka, H. Kuhn, and H. Kronmüller, Phys. Rev. B **49**, 3443 (1994); Th. Schuster, H. Kuhn, E. H. Brandt, M. V. Indenbom, M. Kläser, G. Müller-Vogt, H. U. Habermeier, H. Kronmüller, and A. Forkl, *ibid.* **52**, 10 375 (1995); A. Forkl and H. Kronmüller, *ibid.* **52**, 16 130 (1995).
- ¹⁷M. R. Koblishka, Supercond. Sci. Technol. **9**, 271 (1996).
- ¹⁸T. Schuster, H. Kuhn, and M. V. Indenbom, Phys. Rev. B **52**, 15 621 (1995).
- ¹⁹T. Tamegai, R. Yamada, T. Yasuhira, and T. Shibauchi, in *Critical Currents in Superconductors*, edited by T. Matsushita and K. Yamafuji (World Scientific, Singapore, 1996), p. 125.
- ²⁰T. Schuster, H. Kuhn, M. R. Koblishka, H. Theuss, H. Kronmüller, M. Leghissa, M. Kraus, and G. Saemann-Ischenko, Phys. Rev. B **47**, 373 (1993).
- ²¹M. R. Koblishka, T. H. Johansen, and H. Bratsberg, Supercond. Sci. Technol. **10**, 693 (1997).
- ²²E. H. Brandt and M. V. Indenbom, Phys. Rev. B **48**, 12 893 (1993); E. H. Brandt, *ibid.* **54**, 4246 (1996); Th. Schuster, H. Kuhn, E. H. Brandt, M. V. Indenbom, M. R. Koblishka, and M. Konczykowski, *ibid.* **50**, 16 684 (1994).
- ²³E. Zeldov, J. R. Clem, M. McElfresh, and M. Darwin, Phys. Rev. B **49**, 9802 (1994).
- ²⁴J. McDonald and J. R. Clem, Phys. Rev. B **53**, 8643 (1996).
- ²⁵M. R. Koblishka, T. H. Johansen, H. Bratsberg, L. Püst, A. Galkin, P. Nálevka, M. Maryško, M. Jirsa, M. D. Bentzon, P. Bodin, P. Vase, and T. Freltoft, J. Appl. Phys. **83**, 6798 (1998).
- ²⁶M. R. Koblishka, S. Koishikawa, T. H. Johansen, and M. Murakami (unpublished).